Discontinuity-induced bifurcations in systems with impacts and friction: Discontinuities in the impact law

Arne Nordmark, Harry Dankowicz, Alan Champneys

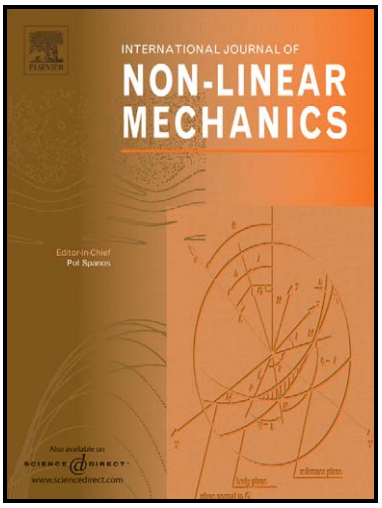

Discontinuity-induced bifurcations in systems with impacts and friction: Discontinuities in the impact law

Arne Nordmark, Harry Dankowicz, Alan Champneys

PII: S0020-7462(09)00090-0
DOI: doi:10.1016/j.ijnonlinmec.2009.05.009
Reference: NLM 1616

www.elsevier.com/locate/nlm

To appear in: *International Journal of Non-Linear Mechanics*

Received date: 27 March 2008
Revised date: 14 May 2009
Accepted date: 30 May 2009

Cite this article as: Arne Nordmark, Harry Dankowicz and Alan Champneys, Discontinuity-induced bifurcations in systems with impacts and friction: Discontinuities in the impact law, *International Journal of Non-Linear Mechanics*, doi:10.1016/j.ijnonlinmec.2009.05.009

Discontinuity-Induced Bifurcations in Systems with Impacts and Friction: Discontinuities in the Impact Law

Arne Nordmark [a] Harry Dankowicz [b] Alan Champneys [c]

[a] *Department of Mechanics, Royal Institute of Technology, S-100 44 Stockholm, Sweden*

[b] *Department of Mechanical Science and Engineering, University of Illinois at Urbana-Champaign, Urbana, IL 61801, USA*

[c] *Department of Engineering Mathematics, University of Bristol, Bristol BS8 1TR, UK*

Abstract

This paper concerns the nonsmooth dynamics of planar mechanical systems with isolated contact in the presence of Coulomb friction. Following Stronge [38], a set of closed-form analytic formulae is derived for a rigid-body impact law based on an energetic coefficient of restitution and a resolution of the impact phase into distinct segments of relative slip and stick. Thus, the impact behavior is consistent both with the assumption of Coulomb friction and with the dissipative nature of impacts. The analysis highlights the presence of boundaries between open regions of initial conditions and parameter values corresponding to distinct forms of the impact law and investigates the smoothness properties of the impact law across these boundaries. It is shown how discontinuities in the impact law are associated with discontinuity-induced bifurcations of periodic trajectories, including nonsmooth folds and persistence scenarios. Numerical analysis of an example mechanical model is used to illustrate and validate the conclusions.

Key words: rigid body mechanics, Coulomb friction, impact, nonsmooth, bifurcation, discontinuities

1 Introduction

There has been much interest in using nonlinear dynamical systems theory to understand the complex behavior of rigid body mechanics in the presence of nonsmooth effects such as dry friction and impact (e.g., [4,25,28,34,38] and

references therein). One difficulty is that the so-called geometric theory of dynamical systems [17,22] typically assumes that the dynamics in question is sufficiently smooth, whereas phenomena such as chattering of impacting systems [5,30] and stick-slip vibrations in the presence of Coulomb friction [35] are fundamental consequences of nonsmoothness. For nonsmooth mechanical systems, even basic questions like existence and uniqueness of solutions to model equations remains an area of active research, and various different formalisms exist, such as sliding modes [14], complementarity [18,37], hybrid systems [36] and differential inclusions [27].

The idea that interaction with discontinuities in a dynamical system can cause qualitative changes in the dynamics has been known for some time, see for example the pioneering work or Feigin [13]. Recently, the present authors and their collaborators have introduced the notion of a *discontinuity-induced bifurcation* as a useful paradigm for explaining dynamical phenomena that are unique to nonsmooth systems. In the context of the dynamics of systems undergoing frictionless impact, Nordmark [29] (see also [15]) introduced the notion of a *discontinuity map* that is able to analytically account for the correction to the smooth dynamics induced by a *grazing* incidence with a discontinuity surface, for which he was able to show the onset of period-adding sequences and chaotic dynamics. Later Dankowicz & Nordmark [6] (see also [8]) generalized the concept to piecewise-smooth continuous models with application to models of dry friction with additional intrinsic degrees of freedom. Di Bernardo *et al.* [12] further derived discontinuity maps for bifurcations unique to discontinuous dynamics that can undergo so-called sliding motion (equivalent to relative stick in the present context of dry friction). Such sliding bifurcations have been shown to underlie the onset of stick-slip oscillations in a variety of models containing dry friction; see Merillas *et al.* [26] for the most comprehensive results to date. These techniques have also been incorporated into numerical software for simulation and parameter continuation [20,33,41]. A comprehensive theory is therefore emerging, as has been summarized in the recent book [9] and review [10], and includes application to models that include both impact and friction, see e.g. [7,40,43].

So far, the case of impacts that involve friction has not been systematically analyzed in the context of discontinuity-induced bifurcation. Note however the work by Leine *et al.* [24], who studied a variant of the classical Painlevé example [31] of a falling rod, albeit with zero coefficient of restitution. There it was shown that passage into the region in which the classical Painlevé paradox applies is associated with bifurcations of branches of equilibria and periodic orbits. Also, Lancioni *et al.* [23] considered simulations of a similar model (which is also closely related to the example introduced in Sec. 2.3 below although with a rather different form of impact law) with a nonzero coefficient of restitution. They found periodic and chaotic motion with intervals of stick and chatter-type motion.

In contrast, the present paper concerns itself in generality with bifurcations of system behavior involving phases of sustained free flight, interrupted by isolated collisional contact events, for which the associated impact laws are piecewise-smooth functions of system parameters and the system state at the onset of contact. Following the approach adopted by Stronge [38] (see also Batlle [1,2] and references therein) in the presence of dry friction, such piecewise-defined impact laws are shown to result from a decomposition of the impact phase into distinct segments of slip and stick motion. Here, the termination of the impact phase is given in terms of the *energetic coefficient of restitution* [38]. Unlike impact laws based on kinematic or kinetic coefficients of restitution, this approach is guaranteed to lead to dissipative collisions in all cases (see the discussion in Sec. 6 below for more details).

The key point of the paper is that discontinuity-induced bifurcations can occur due to the inherent nonsmoothness of the impact law across well-defined boundaries associated with changes in the sequence of stick and slip segments during the impact phase. As shown in Sec. 5, such changes result in at-most piecewise-smooth Poincaré mappings on neighborhoods of degenerate periodic trajectories. Specifically, mappings with a discontinuity in the first derivative are known to be associated with a catastrophic loss of stable motion and sudden jumps between different kinds of attractor, see [9,10,13] and Figs. 6 and7 below.

The paper is organized as follows. Section 2 reviews the Lagrangian framework for impulsive contact at isolated points on a rigid-body mechanism and illustrates the formalism for an example system. A collection of impact mappings relating incoming and outgoing relative velocities are derived in Sec. 3. Boundaries between open regions of initial conditions and parameter values corresponding to distinct forms of the impact mappings are enumerated in Sec. 4 as are the smoothness properties of the corresponding impact law across these boundaries. Section 5 goes on to study the different kinds of discontinuity-induced bifurcations that arise from the various degrees of nonsmoothness in the impact law, and to provide support for these conclusions using numerical analysis of the example mechanism. The paper ends with a discussion that puts the results into the context of previous work and provides an outlook to subsequent work.

2 Mechanical model

2.1 A Lagrangian formulation

Consider a multibody mechanism whose configuration relative to an inertial reference frame may be described in terms of a column matrix q of generalized coordinates and (possibly) the time coordinate t. Its dynamics are then governed by Lagrange's equations

$$\frac{d}{dt}\left(\partial_{\dot{q}} T\right) - \partial_q T = F, \tag{1}$$

where the components of the row matrices $\partial_q T$ and $\partial_{\dot{q}} T$ are the partial derivatives of the kinetic energy T with respect to the generalized coordinates and the generalized velocities, respectively, and where F denotes a row matrix of generalized forces.

Suppose that contact occurs between a point P on the multibody mechanism and a rigid element in its environment. Throughout the duration of contact, let $F = F_c + F_a$, where F_c represents the generalized forces associated with contact interactions and F_a represents all other generalized forces acting on the mechanism. Denote by $x\left(q,t\right)$ the transformation from the generalized coordinates to the column matrix of Cartesian coordinates of the point P relative to the inertial reference frame. It follows that

$$F_c = \lambda \cdot \partial_q x \tag{2}$$

for some row matrix λ.

There exists a positive definite, symmetric matrix M, whose entries are functions of q and t, such that

$$T = \frac{1}{2}\dot{q}^T \cdot M \cdot \dot{q} + \ldots,$$

where the omitted terms are at most linear in the column matrix of generalized velocities $\dot{q}$. From (1) and (2) it follows that

$$\ddot{q} = M^{-1} \cdot \left(\partial_q x\right)^T \cdot \lambda^T + \ldots, \tag{3}$$

where the omitted terms are independent of λ and are a function of F_a, q, $\dot{q}$, and t only. Finally, denote by $v = \partial_q x \cdot \dot{q} + \partial_t x$ the velocity of the point P relative to the inertial frame. In terms of the symmetric matrix

$$m^{-1} = \partial_q x \cdot M^{-1} \cdot \left(\partial_q x\right)^T, \tag{4}$$

it then follows that

$$\dot{v} = m^{-1} \cdot \lambda^T + \ldots, \tag{5}$$

where the omitted terms are independent of λ and are a function of F_a, q, $\dot{q}$, and t only.

In the case of motion constrained to a plane,

$$\partial_q x = \begin{pmatrix} c_T \\ c_N \end{pmatrix}, \quad v = \begin{pmatrix} v_T \\ v_N \end{pmatrix}, \quad \lambda = (\lambda_T, \lambda_N),$$

where the subscripts $_T$ and $_N$ refer to components tangential and normal to the common tangent direction at P, respectively. Suppose that $\partial_q x$ has full row rank (which would not be the case for the model considered in [23,24] at points where $\phi = \pm\pi/2$). From (4) it follows that

$$m^{-1} = \begin{pmatrix} A & B \\ B & C \end{pmatrix}$$

is positive definite, i.e., that

$$A > 0, \quad C > 0, \quad AC - B^2 > 0. \tag{6}$$

The formulation (1), (2) allows for several different modes of sustained motion on open non-zero intervals of time. Let x_N be a coordinate representing the normal distance between P and the rigid element, such that sustained free motion (with $\lambda = 0$) occurs whenever $x_N > 0$ for such a time interval. Assume that normal contact interactions acting at P are *compressive*, i.e., that $\lambda_N \geq 0$ and that $\lambda_N = 0$ when there is no contact at P. Furthermore, suppose that the simple Amonton-Coulomb friction law

$$|\lambda_T| \leq \mu \lambda_N \tag{7}$$

applies at P for some non-negative physical constant μ, representing a *coefficient of friction*. Sustained contact then occurs on intervals for which $x_N \equiv 0$ and $\lambda_N > 0$. In particular, we distinguish between sustained stick where, in addition to (7), the relative velocity between P and the instantaneous point of contact on the rigid element vanishes; and sustained slip, where equality occurs in (7). This work shall not consider the dynamics of sustained contact, but shall instead treat impulsive contact, or impact, which occurs at isolated points of time separating open intervals of free flight.

2.2 Impulsive contact

Suppose that contact is initiated between P and a point P' on the rigid element at some time t_0, such that $x_{N,0} = 0$ and $v_{N,0} < 0$, where the subscript $_0$ represents evaluation at $t = t_0$. By the standard impact approximation, suppose that there exists an $\mathcal{O}(\varepsilon)$ interval of time following t_0 for some $\varepsilon \ll 1$, referred to below as the *impact phase*, during which i) the rigidity constraint is only approximately satisfied, ii) $F_a, \varepsilon\lambda, \dot{q} = \mathcal{O}(1)$, and iii) the position and velocity of P' relative to the inertial frame change by $\mathcal{O}(\varepsilon)$. Let $t - t_0 = \varepsilon\tilde{t}$ and $\varepsilon\lambda = \tilde{\lambda}$. It follows from (3) and (5) that

$$\frac{d\dot{q}}{d\tilde{t}} = \left(M^{-1}\right)_0 \cdot (\partial_q x)_0^T \cdot \tilde{\lambda}^T + \mathcal{O}(\varepsilon) \tag{8}$$

and

$$\frac{dv}{d\tilde{t}} = \left(m^{-1}\right)_0 \cdot \tilde{\lambda}^T + \mathcal{O}(\varepsilon), \tag{9}$$

where, without loss of generality, v can be taken to represent the relative velocity between P and P' during the impact phase.

Neglecting $\mathcal{O}(\varepsilon)$ terms, it follows from (8) and (9) that

$$\Delta\dot{q} = \left(M^{-1}\right)_0 \cdot (\partial_q x)_0^T \cdot m_0 \cdot \Delta v \tag{10}$$

is the total change in the generalized velocities during the impact phase. In what follows, we shall refer to a relationship that yields $v_0 \mapsto v_0 + \Delta v$ as an *impact mapping* and to $(q_0, \dot{q}_0) \mapsto (q_0, \dot{q}_0 + \Delta\dot{q})$ as the resultant *impact law*.

During the impact phase, the *normal impulse* p is a monotonically increasing $\mathcal{O}(1)$ function of $\tilde{t}$, since $p(t_0) = 0$ and $dp/d\tilde{t} = \tilde{\lambda}_N > 0$. If we replace $\tilde{t}$ by p as independent variable, drop tildes, and neglect $\mathcal{O}(\varepsilon)$ terms, we finally obtain

$$\frac{dv}{dp} = \frac{1}{\lambda_N}\left(m^{-1}\right)_0 \cdot \lambda^T \tag{11}$$

(cf. [2,19,38]) for the rate of change of the relative velocity as a function of the normal impulse during the impact phase.

2.3 A model example

The theory in this paper shall be applied to an example system that is a generalisation of the model problem studied by Leine *et al.* [24] and Lancioni *et al.* [23] and is related to the original Painlevé problem [31] of a rod falling on a hard surface.

Consider the planar motion of a homogeneous rod of unit mass and twice unit length in the presence of a unilateral constraint corresponding to the non-penetrability of a half-plane that is stationary relative to an inertial reference frame. Denote by P_1 and P_2 the two end points of the rod and restrict attention to the case of possible contact of P_1 with the straight-line boundary of the stationary half-plane (cf. Fig. 1).

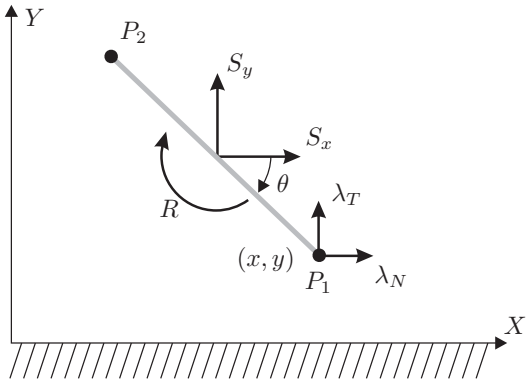

Fig. 1. Sketch of the model example.

Let $x = q_1$ and $y = q_2$ be the Cartesian coordinates of P_1 relative to the coordinate axes shown in Fig. 1. Moreover, let $\theta = q_3$ denote the counter-clockwise angle of rotation required to align the rod with the X axis, with P_2 to the left of P_1. It follows that

$$T = \frac{\dot{x}^2}{2} + \frac{\dot{y}^2}{2} + (\dot{x}\sin\theta + \dot{y}\cos\theta)\,\dot{\theta} + \frac{2}{3}\dot{\theta}^2,$$

$c_T = (1, 0, 0)$, and $c_N = (0, 1, 0)$. Let S_x and S_y be the components along the X and Y axes of the net external force (excluding contact forces) acting on the rod. Similarly, let R denote the net external torque (excluding contact forces) acting about the center of mass of the rod, such that

$$F_a = (S_x, S_y, R + S_x\sin\theta + S_y\cos\theta)\,.$$

It follows that the equations of motion become

$$\begin{aligned}
\ddot{x} &= S_x - 3R\sin\theta - \dot{\theta}^2\cos\theta + \left(1 + 3\sin^2\theta\right)\lambda_T + 3\sin\theta\cos\theta\lambda_N \\
\ddot{y} &= S_y - 3R\cos\theta + \dot{\theta}^2\sin\theta + 3\sin\theta\cos\theta\lambda_T + \left(1 + 3\cos^2\theta\right)\lambda_N \\
\ddot{\theta} &= 3R - 3\cos\theta\lambda_N - 3\sin\theta\lambda_T.
\end{aligned}$$

Moreover, in the notation of (6)

$$A = 1 + 3\sin^2\theta, \quad B = 3\sin\theta\cos\theta, \quad C = 1 + 3\cos^2\theta. \tag{12}$$

3 The impact phase

3.1 An energetic impact law

Consider the equations (11) written in terms of tangential and normal components

$$\frac{dv_T}{dp} = A\frac{\lambda_T}{\lambda_N} + B, \qquad \frac{dv_N}{dp} = B\frac{\lambda_T}{\lambda_N} + C, \tag{13}$$

where we have dropped the $_0$ subscript on A, B, and C for notational convenience. The assumption of the Amonton-Coulomb-type model of dry friction enables us to distinguish between three modes of impulsive contact motion: *positive slip* for which

$$v_T > 0 \text{ and } \lambda_T = -\mu\lambda_N,$$

negative slip for which

$$v_T < 0 \text{ and } \lambda_T = \mu\lambda_N,$$

and *stick* for which

$$v_T = \dot{v}_T = 0 \text{ and } |\lambda_T| \leq \mu\lambda_N.$$

In particular, it follows from (13) that stick motion is persistent with

$$\lambda_T = -\frac{B}{A}\lambda_N$$

provided that

$$|B| - \mu A \leq 0.$$

Indeed, in this case, $v_T = 0$ is stable against perturbations in initial conditions.

Given these three conditions, the dynamics of (13) is now described by a concatenation of several different trajectory segments in the (v_T, v_N) plane such that

$$\frac{dv_T}{dp} = k_T, \quad \frac{dv_N}{dp} = k_N, \tag{14}$$

where the *rate constants* are:

$$k_T = k_T^+ \stackrel{\text{def}}{=} B - \mu A, \qquad k_N = k_N^+ \stackrel{\text{def}}{=} C - \mu B$$

in positive slip;

$$k_T = k_T^- \stackrel{\text{def}}{=} B + \mu A, \qquad k_N = k_N^- \stackrel{\text{def}}{=} C + \mu B$$

in negative slip; and

$$k_T = k_T^0 \stackrel{\text{def}}{=} 0, \qquad k_N = k_N^0 \stackrel{\text{def}}{=} \frac{AC - B^2}{A} > 0$$

in stick. Since

$$k_N^{\pm} = k_N^0 + \frac{B}{A} k_T^{\pm},$$

it follows that the two rate constants corresponding to a given slip segment cannot vanish simultaneously. Eq. (14) yields the first integral

$$k_N v_T - k_T v_N = \text{constant} \tag{15}$$

referred to below as the *trajectory integral*. It follows that trajectory segments in the (v_T, v_N) plane lie along straight lines (cf. Fig. 3 below).

The impact phase can be decomposed into two separate processes, viz., an initial *compression phase* for which $v_N < 0$, followed by a *restitution phase* for which $v_N \geq 0$. The impact mapping that yields Δv_T and Δv_N as functions of the initial values of v_T, v_N, A, B, and C will then be defined by the values of v_T and v_N at the terminal point of the restitution phase. In the energetic impact process [38], the restitution phase is assumed to terminate when the total mechanical work performed by the normal force during restitution equals $-r^2$ times the total mechanical work performed by the normal force during compression, for some constant $r \in [0, 1]$ referred to as the *energetic coefficient of restitution*. That is,

$$\int_{v_N<0} v_N dp = -r^2 \int_{v_N>0} v_N dp. \tag{16}$$

From (14) it follows that

$$v_N = \frac{v_N}{k_N} \frac{dv_N}{dp} = \frac{d}{dp} \left(\frac{v_N^2}{2k_N} \right) \tag{17}$$

provided that $k_N \neq 0$ or, equivalently, that

$$v_N = \frac{v_N}{k_T} \frac{dv_T}{dp} = \frac{d}{dp} \left(\frac{(2k_T v_N - k_N v_T)\, v_T}{2k_T^2} \right),$$

provided that $k_T \neq 0$. As will shortly be shown, individual trajectory itineraries (sequences of stick or slip) during impact depend on the initial conditions at the onset of the impact phase. For the time being, suppose that the compression phase consists of n_c trajectory segments and that the restitution phase consists of n_r segments. Denote by $v_{N,i-1}$ and $v_{N,i}$ the values of the normal velocity at the beginning and end, respectively, of the i-th impact phase segment and let $k_{N,i}$ denote the corresponding rate constant (here taken to be nonzero). Then, using (17), the work balance condition (16) becomes

$$\sum_{i=n_c+1}^{n_c+n_r} \frac{v_{N,i}^2 - v_{N,i-1}^2}{2k_{N,i}} = -r^2 \sum_{i=1}^{n_c} \frac{v_{N,i}^2 - v_{N,i-1}^2}{2k_{N,i}}. \tag{18}$$

In particular, n_r and n_c must both be greater than or equal to 1 and the value of the normal velocity at the termination of the impact phase is greater than or equal to zero with equality only in the case when $r = 0$.

Before proceeding to the general case, consider for the moment the special case of a perfectly smooth surface with $\mu = 0$ and a collision with $B \neq 0$, so that sticking motion is not possible and there is no distinction between slip in either direction. Therefore, since there is only one mode of motion, we must have $n_c = 1$ and $n_r = 1$, such that $v_{N,1} = 0$ at the end of the first segment. Equations (15) and (18) then become

$$Cv_{T,1} = Cv_{T,0} - Bv_{N,0}, \quad Cv_{T,2} - Bv_{N,2} = Cv_{T,1}$$

and

$$\frac{v_{N,2}^2}{2C} = -r^2 \frac{-v_{N,0}^2}{2C}.$$

It follows that

$$(v_{T,2}, v_{N,2}) = \left(v_{T,0} - \frac{B}{C}(1+r)\, v_{N,0}, -rv_{N,0} \right),$$

i.e.,

$$(\Delta v_T, \Delta v_N) = (v_{T,2}, v_{N,2}) - (v_{T,0}, v_{N,0}) = -\left(\frac{B}{C}, 1\right)(1+r)\, v_{N,0}.$$

Clearly, in the limit of no coupling between the impulsive normal and tangential dynamics, i.e., for $B \to 0$, the impact mapping reduces to the Newtonian restitution rule $(v_{T,0}, v_{N,0}) \mapsto (v_{T,0}, -rv_{N,0})$.

Unless otherwise stated, it is assumed that $\mu > 0$ in what follows. In this case, the equality

$$(C - \mu B)(\mu A + B) + (C + \mu B)(\mu A - B) = 2\mu \left(AC - B^2 \right)$$

implies that at most one of the four quantities k_N^+, k_N^-, k_T^-, and $-k_T^+$ is non-positive.

3.2 Explicit impact mappings

Consider the rescaling

$$\frac{d}{dp} \to -\frac{C}{v_{N,0}} \frac{d}{dp}, \quad v_T \to -v_{N,0} \sqrt{\frac{A}{C}} v_T, \quad v_N \to -v_{N,0} v_N,$$

$$B \to \sqrt{AC} B, \quad \mu \to \sqrt{\frac{C}{A}} \mu,$$

where $v_{N,0} < 0$ is the value of the normal velocity at the beginning of the impact phase. The impact phase dynamics in the (v_T, v_N) plane again correspond to a dynamical system of the form (14), where $|B| < 1$, stick persists only if $|B| \leq \mu$ and $A = C = -v_{N,0} = 1$.

As shown in Fig. 2, in terms of the rescaled parameters the four curves $B = \pm\mu$ and $B = \pm\mu^{-1}$ separate the strip $|B| < 1$, $\mu > 0$ in the (B, μ) plane into five open sets corresponding to distinct sign combinations of the rate constants in positive and negative slip. Panels (a)-(e) of Fig. 3 depict a representative sample of the corresponding impact phases in the (v_T, v_N)-plane. Initial conditions for which $v_T > 0$ and $k_N^+ < 0$ (region 5 in panel (b)) and $v_T < 0$ and $k_N^- < 0$ (region 6 in panel (c)) correspond to cases where the Painlevé paradox occurs for positive slip. This phenomenon, which is also referred to as jam [38], means that negative initial normal velocities become further negative, since $dv_N/dp < 0$ during the initial compression phase. Also, initial conditions for which $k_T^+ > 0$ or $k_T^- < 0$ (panels (d) and (e) in Fig. 3) correspond to $|B| > \mu$ and the absence of impulsive stick motion.

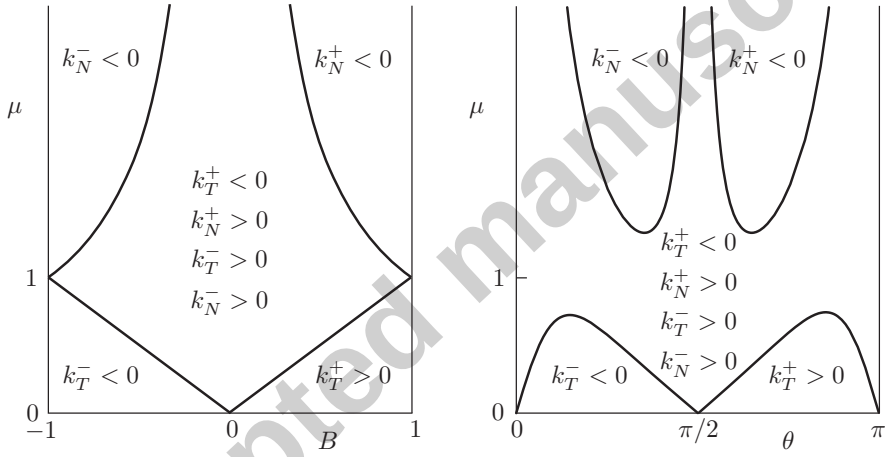

Fig. 2. The five different allowable sign combinations of $k_T^\pm$ and $k_N^\pm$ (all signs are assumed to be the same as in the central region unless otherwise stated) as parametrized by the rescaled variables B and μ (left panel) and by the unscaled variables θ and μ in the model example (right panel) in Sec. 2.3.

It is straightforward to see from Fig. 3 that the impact phase is described by one of three possible cases differentiated by the number of segments in compression and restitution and the corresponding impulsive modes.

Case I: Let $\mathbf{g}_I : (v_{T,0}, v_{N,0}, k_T, k_N, r) \mapsto (v_{T,2}, v_{N,2})$ represent the impact mapping corresponding to a single-mode impact phase consisting of a single compression segment followed by a single restitution segment both with rate constants k_T and $k_N \neq 0$. In this case, at the terminal point of the first segment $v_{N,1} = 0$. Simultaneous solution of the work balance equation (18)

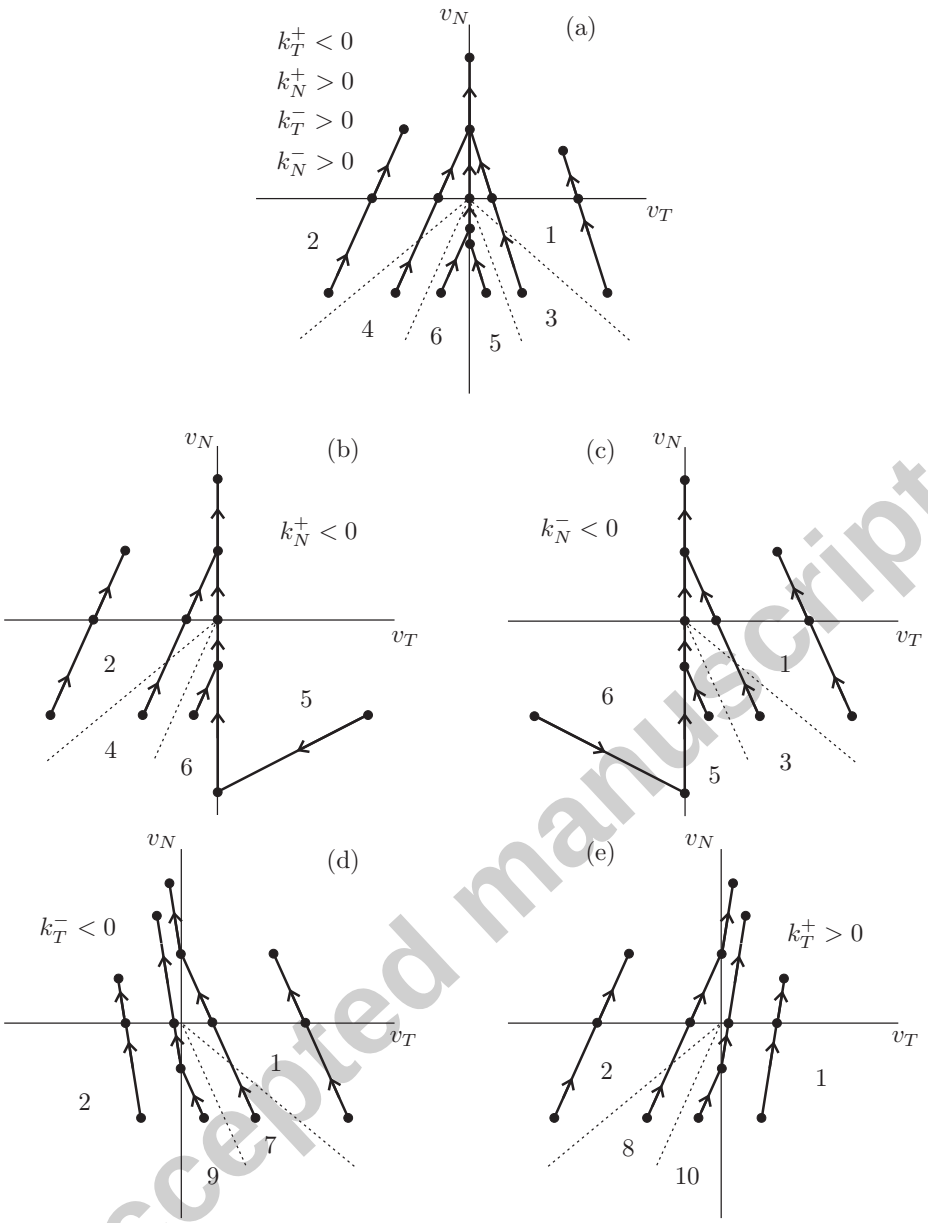

Fig. 3. The flow of the impacting phase projected onto the (v_T, v_N)-plane for each of the five cases represented by open regions in Fig. 2. Dashed lines represent the boundaries between the ten regions of initial conditions.

and the trajectory integral (15) for each of the two segments then yields

$$v_{T,2} = v_{T,0} - (1+r)\,\frac{k_T}{k_N} v_{N,0},$$
$$v_{N,2} = -r v_{N,0}.$$

Case II: Let $\mathbf{g}_{II} : (v_{T,0}, v_{N,0}, k_T, k_N, k'_T, k'_N, r) \mapsto (v_{T,3}, v_{N,3})$ represent the

impact mapping corresponding to a two-mode impact phase consisting of a single compression segment followed by two restitution segments with rate constants $k_T \neq 0$ and $k_N \neq 0$ for the first two segments and k'_T and $k'_N \neq 0$ for the last segment. In this case, at the terminal point of the first segment $v_{N,1} = 0$. Similarly, at the terminal point of the second segment $v_{T,2} = 0$. Simultaneous solution of the work balance equation (18) and the trajectory integral (15) for each of the three segments then yields

$$v_{T,3} = \frac{k'_T}{k'_N}\left(\frac{k_N}{k_T}v_{T,0} - v_{N,0} + \sqrt{\left(1-\frac{k'_N}{k_N}\right)\left(\frac{k_N}{k_T}v_{T,0} - v_{N,0}\right)^2 + r^2\frac{k'_N}{k_N}v_{N,0}^2}\right),$$
$$v_{N,3} = \sqrt{\left(1-\frac{k'_N}{k_N}\right)\left(\frac{k_N}{k_T}v_{T,0} - v_{N,0}\right)^2 + r^2\frac{k'_N}{k_N}v_{N,0}^2}.$$

Case III: Let $\mathbf{g}_{III} : (v_{T,0}, v_{N,0}, k_T, k_N, k'_T, k'_N, r) \mapsto (v_{T,3}, v_{N,3})$ represent the impact mapping corresponding to a two-mode impact phase consisting of two compression segments followed by a single restitution segment with rate constants $k_T \neq 0$ and k_N for the first segment and k'_T and $k'_N \neq 0$ for the last two segments. In this case, at the terminal point of the first segment $v_{T,1} = 0$. Similarly, at the terminal point of the second segment $v_{N,2} = 0$. Simultaneous solution of the work balance equation (18) and the trajectory integral (15) for each of the three segments then yields

$$v_{T,3} = \frac{k'_T}{k'_N}\left(\frac{k_N}{k_T}v_{T,0} - v_{N,0} + r\sqrt{\left(1-\frac{k'_N}{k_N}\right)\left(\frac{k_N}{k_T}v_{T,0} - v_{N,0}\right)^2 + \frac{k'_N}{k_N}v_{N,0}^2}\right),$$
$$v_{N,3} = r\sqrt{\left(1-\frac{k'_N}{k_N}\right)\left(\frac{k_N}{k_T}v_{T,0} - v_{N,0}\right)^2 + \frac{k'_N}{k_N}v_{N,0}^2},$$

provided that $k_N \neq 0$ and

$$v_{T,3} = 0,$$
$$v_{N,3} = r\sqrt{v_{N,0}^2 + \frac{2k'_N v_{T,0} v_{N,0}}{k_T}},$$

provided that $k_N = 0$ (in which case $k'_T = 0$).

Table 1 shows the values of k_T, k_N, k'_T, and k'_N and the corresponding impact mapping for each of the ten labeled regions in panels (a)-(e) in Fig. 3.

The above analysis assumes that $r > 0$, in which case free motion ensues after the impact phase. As $r \to 0$, regions 3, 4, 7, and 8 disappear, leaving only impact phases governed by the impact mappings $\mathbf{g}_I$ and $\mathbf{g}_{III}$, respectively.

Region	k_T	k_N	k'_T	k'_N	Impact mapping
1	k_T^+	k_N^+	$*$	$*$	$\mathbf{g}_I$
2	k_T^-	k_N^-	$*$	$*$	$\mathbf{g}_I$
3	k_T^+	k_N^+	k_T^0	k_N^0	$\mathbf{g}_{II}$
4	k_T^-	k_N^-	k_T^0	k_N^0	$\mathbf{g}_{II}$
5	k_T^+	k_N^+	k_T^0	k_N^0	$\mathbf{g}_{III}$
6	k_T^-	k_N^-	k_T^0	k_N^0	$\mathbf{g}_{III}$
7	k_T^+	k_N^+	k_T^-	k_N^-	$\mathbf{g}_{II}$
8	k_T^-	k_N^-	k_T^+	k_N^+	$\mathbf{g}_{II}$
9	k_T^+	k_N^+	k_T^-	k_N^-	$\mathbf{g}_{III}$
10	k_T^-	k_N^-	k_T^+	k_N^+	$\mathbf{g}_{III}$

Table 1
Values of the rate constants and the impact map type for the 10 different regions.

Indeed,

$$\lim_{r\to 0} \mathbf{g}_I\left(v_{T,0}, v_{N,0}, k_T, k_N, r\right) = \mathbf{g}_I\left(v_{T,0}, v_{N,0}, k_T, k_N, 0\right) = \left(v_{T,0}, 0\right)$$

and

$$\begin{aligned}\lim_{r\to 0} \mathbf{g}_{III}\left(v_{T,0}, v_{N,0}, k_T, k_N, k'_T, k'_N, r\right) &= \mathbf{g}_{III}\left(v_{T,0}, v_{N,0}, k_T, k_N, k'_T, k'_N, 0\right) \\ &= \left(\frac{k'_T}{k'_N}\left(\frac{k_N}{k_T} v_{T,0} - v_{N,0}\right), 0\right)\end{aligned}$$

consistent with the expectation that the normal velocity at the terminal point of the restitution phase should vanish in this *plastic* limit (cf. Brogliato *et al.* [24]).

4 Smoothness of the impact law

We proceed to enumerate codimension-one boundaries between collections of initial conditions corresponding to distinct forms of the impact law and to investigate the degree of smoothness of the impact law across these boundaries.

4.1 Boundaries

For a fixed value of $r = 0.9$, Figure 4 gives a complete picture of the 10 regions and their boundaries in terms of the scaled variables. In fact, a careful examination of the various formulae involved shows that the r dependence is quite simple and does not change the topology of these diagrams, as long as $r > 0$. The figure suggests the procedure shown in Fig. 5 for deciding the region corresponding to any given initial conditions and parameter values.

We identify five distinct types of codimension-one boundaries in the impact law. In particular, initial conditions on the boundaries between regions 2 and 4, between 1 and 3, between 2 and 8, and between 1 and 7, respectively, correspond to a *Case I* impact phase with rate constants k_T and k_N and $v_{T,2} = 0$ or a *Case II* impact phase with rate constants k_T, k_N, k'_T, and k'_N and a zero-length terminal segment. In either case, these are characterized by a zero tangential velocity at the terminal point of the impact phase and, consequently, that

$$k_N v_{T,0} - (1 + r)\, k_T v_{N,0} = 0.$$

Similarly, initial conditions on the boundaries between regions 4 and 6, between 3 and 5, between 8 and 10, and between 7 and 9, respectively, correspond to a *Case II* or *Case III* impact phase with rate constants k_T, k_N, k'_T, and k'_N, $v_{T,1} = 0$, and a zero-length middle segment. In either case, these are characterized by a zero tangential velocity at the terminal point of the compression phase and, consequently, that

$$k_N v_{T,0} - k_T v_{N,0} = 0.$$

Initial conditions on the boundaries between regions 1 and 10 and between 2 and 9, respectively, correspond to a *Case I* impact phase with rate constants k'_T and k'_N or *Case III* impact phase with rate constants k_T, k_N, k'_T, and k'_N and zero-length initial segment. Similarly, initial conditions on the boundaries between regions 5 and 6, correspond to a *Case III* impact phase with rate constants k_T^+, k_N^+, k_T^0, and k_N^0 or *Case III* impact phase with rate constants k_T^-, k_N^-, k_T^0, and k_N^0 with $v_{T,1} = 0$ and zero-length initial segments. In either case, these are characterized by a zero tangential velocity at the beginning of the impact phase, i.e., that

$$v_{T,0} = 0.$$

Finally, initial conditions on the boundaries between regions 3 and 7, between 5 and 9, between 4 and 8, and between 6 and 10 respectively, correspond to a *Case II* (or *Case III*) impact phase with rate constants k_T, k_N, k'_T, and k'_N or an impact phase of the same case with rate constants k_T, k_N, 0, and k_N^0. In either case, these are characterized by the vanishing of the tangential rate

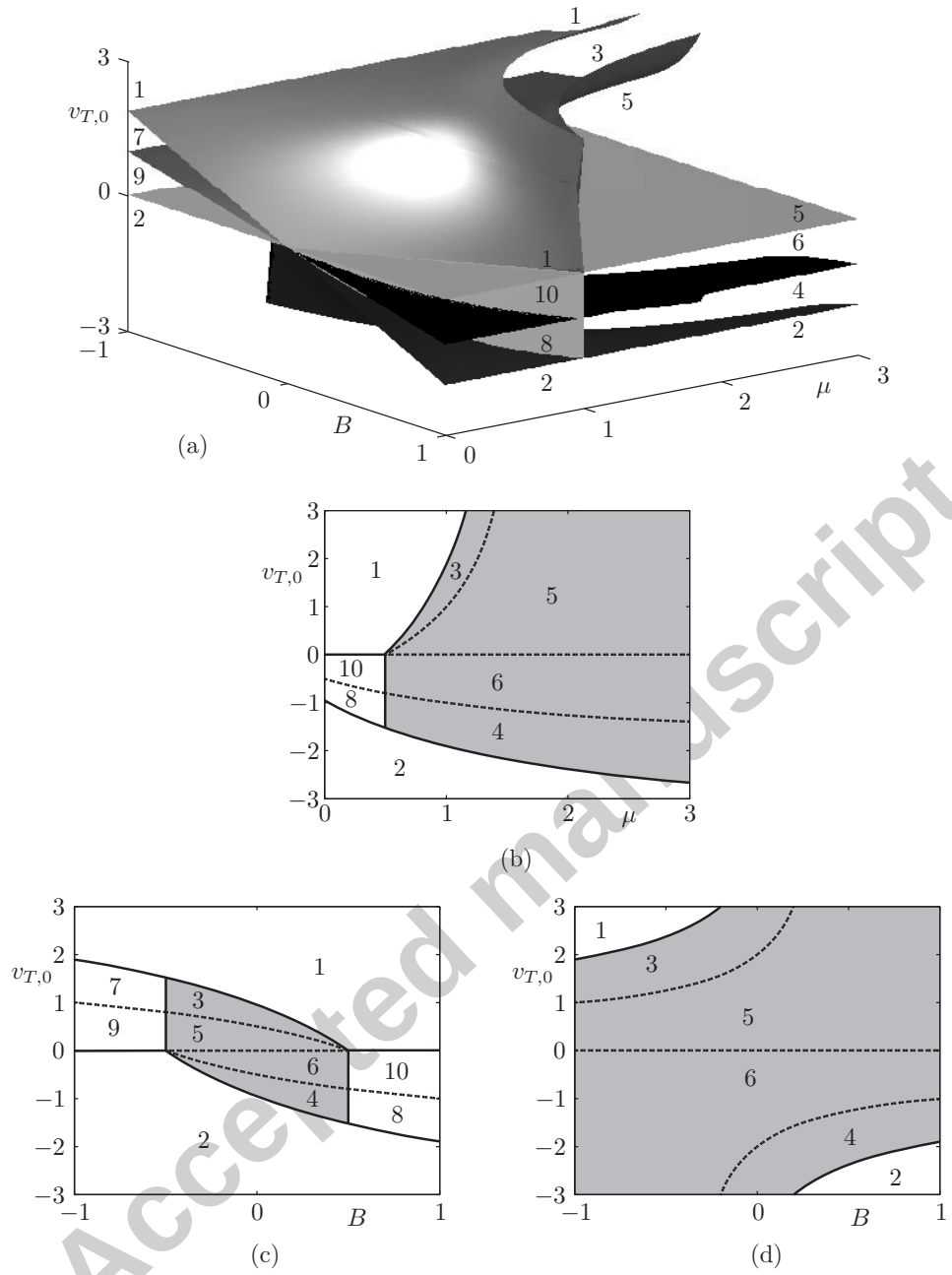

Fig. 4. The boundary structure for $r = 0.9$ in terms of the rescaled parameters. (a) Full view. The boundaries between regions 3 and 7 and between 5 and 9 are obscured. (b) Section for $B = 0.5$. (c) Section for $\mu = 0.5$. (d) Section for $\mu = 2$. Here, solid curves represent boundaries with C^0 continuity, dashed curves represent boundaries with C_1 continuity, and shading is used to highlight the regions for which the impact phase ends in impulsive stick and for which the impact law is co-rank 1.

constant for the last two trajectory segments, i.e., that

$$k'_T = 0.$$

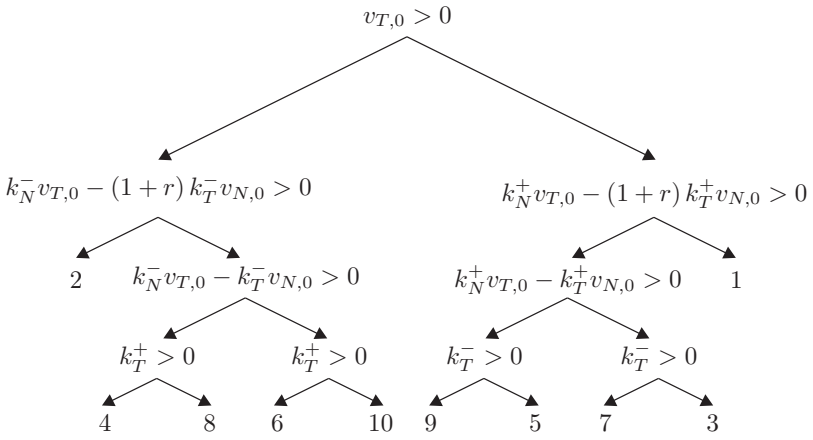

Fig. 5. Decision tree on the initial conditions at the start of an impact phase that determines the region. The branches to the right are taken when the condition is fulfilled.

4.2 Discontinuities

For each of the codimension-one boundaries identified in Sec. 4.1 we derive an explicit expression for the change in the impact law as the boundary is crossed in order to analyse the smoothness of the impact law at that point. For notational convenience, let $z = (q, \dot{q})^T$ in what follows. The five cases can be summarised as follows:

$v_T = 0$ **at end of impact phase:** Consider initial conditions on the boundaries between regions 2 and 4, between 1 and 3, between 2 and 8, and between 1 and 7, respectively, i.e., such that $k_N v_{T,0} - (1+r)\, k_T v_{N,0} = 0$. For nearby initial conditions, Taylor expansion yields

$$\delta\left[\mathbf{g}_{II}\left(v_T, v_N, k_T, k_N, k_T', k_N', r\right) - \mathbf{g}_I\left(v_T, v_N, k_T, k_N, r\right)\right] = \left[\left(\frac{k_T' - k_T}{k_T k_N}, \frac{k_N' - k_N}{k_T k_N}\right) + \mathcal{O}\left(\delta z\right)\right] \delta\left(k_N v_T - (1+r)\, k_T v_N\right), \quad (19)$$

i.e., the impact law is only $\mathcal{C}^0$ under variations in $k_N v_T - (1+r)\, k_T v_N$ across this boundary.

$v_T = 0$ **at end of compression phase:** Consider, instead, initial conditions on the boundaries between regions 4 and 6, between 3 and 5, between 8 and 10, and between 7 and 9, respectively, i.e., such that $k_N v_{T,0} - k_T v_N = 0$.

For nearby initial conditions, Taylor expansion yields

$$\delta\left[\mathbf{g}_{III}\left(v_T, v_N, k_T, k_N, k'_T, k'_N, r\right) - \mathbf{g}_{II}\left(v_T, v_N, k_T, k_N, k'_T, k'_N, r\right)\right] = \left[\frac{\left(k_N - k'_N\right)\sqrt{\frac{k'_N}{k_N}}\left(1-r^2\right)^2}{2k_T^2 k_N'^2 r v_N}\left(k'_T, 1\right) + \mathcal{O}\left(\delta z\right)\right]\delta\left[\left(k_N v_T - k_T v_N\right)\right]^2,$$

i.e., the impact law is only $\mathcal{C}^1$ under variations in $k_N v_T - k_T v_N$ across this boundary.

$v_T = 0$ **at impact; no stick:** Now consider initial conditions on the boundaries between regions 1 and 10 and between 2 and 9, respectively, i.e., such that $v_{T,0} = 0$. For nearby initial conditions, Taylor expansion yields

$$\delta\left[\mathbf{g}_{I}\left(v_T, v_N, k'_T, k'_N, r\right) - \mathbf{g}_{III}\left(v_T, v_N, k_T, k_N, k'_T, k'_N, r\right)\right] = \left[\left(1 - \frac{k'_T k_N}{k_T k'_N} - \frac{k'_T}{k'_N}\frac{\left(k_N - k'_N\right)r}{k_T}, \frac{\left(k'_N - k_N\right)r}{k_T}\right) + \mathcal{O}\left(\delta z\right)\right]\delta v_T,$$

i.e., the impact law is only $\mathcal{C}^0$ under variations in v_T across this boundary.

$v_T = 0$ **at impact; stick:** Similarly, consider initial conditions on the boundaries between regions 5 and 6, such that $v_{T,0} = 0$. For nearby initial conditions, Taylor expansion yields

$$\delta\left[\mathbf{g}_{III}\left(v_T, v_N, k_T^+, k_N^+, k_T^0, k_N^0, r\right) - \mathbf{g}_{III}\left(v_T, v_N, k_T^-, k_N^-, k_T^0, k_N^0, r\right)\right] = \left(0, -\frac{\left(k_T^+ + k_T^-\right)k_N^0 r\mu}{2v_N k_T^+ k_T^-} + \mathcal{O}\left(\delta z\right)\right)\left(\delta v_T\right)^2,$$

i.e., the impact law is only $\mathcal{C}^1$ under variations in v_T across this boundary.

Loss of stick phase: Finally, consider initial conditions on the boundaries between regions 3 and 7, between 5 and 9, between 4 and 8, and between 6 and 10 respectively, i.e., such that $k'_T = 0$. Recall that

$$k'_N = k_N^0 + \frac{B}{A}k'_T.$$

For nearby initial conditions, Taylor expansion then yields

$$\delta\left[\mathbf{g}_{II}\left(v_T, v_N, k_T, k_N, k_T', k_N^0 + \frac{B}{A}k_T', r\right) - \mathbf{g}_{II}\left(v_T, v_N, k_T, k_N, 0, k_N^0, r\right)\right] = \left[\left(\frac{1}{k_N^0}\left(\frac{k_N}{k_T}v_T - v_N + \sqrt{\left(1 - \frac{k_N^0}{k_N}\right)\left(\frac{k_N}{k_T}v_T - v_N\right)^2 + r^2\frac{k_N^0}{k_N}v_N^2}\right),\right.\right.$$
$$\left.\left.\frac{B}{A}\frac{\frac{1}{k_N}\left(-\left(\frac{k_N}{k_T}v_T - v_N\right)^2 + r^2v_N^2\right)}{2\sqrt{\left(1 - \frac{k_N^0}{k_N}\right)\left(\frac{k_N}{k_T}v_T - v_N\right)^2 + r^2\frac{k_N^0}{k_N}v_N^2}}\right) + \mathcal{O}(\delta z)\right]\delta k_T'$$

or

$$\delta\left[\mathbf{g}_{III}\left(v_T, v_N, k_T, k_N, k_T', k_N^0 + \frac{B}{A}k_T', r\right) - \mathbf{g}_{III}\left(v_T, v_N, k_T, k_N, 0, k_N^0, r\right)\right] = \left[\left(\frac{1}{k_N^0}\left(\frac{k_N}{k_T}v_T - v_N + r\sqrt{\left(1 - \frac{k_N^0}{k_N}\right)\left(\frac{k_N}{k_T}v_T - v_N\right)^2 + \frac{k_N^0}{k_N}v_N^2}\right),\right.\right.$$
$$\left.\left.\frac{B}{A}\frac{\frac{r}{k_N}\left(-\left(\frac{k_N}{k_T}v_T - v_N\right)^2 + v_N^2\right)}{2\sqrt{\left(1 - \frac{k_N^0}{k_N}\right)\left(\frac{k_N}{k_T}v_T - v_N\right)^2 + \frac{k_N^0}{k_N}v_N^2}}\right) + \mathcal{O}(\delta z)\right]\delta k_T', \quad (20)$$

i.e., the impact law is only $\mathcal{C}^0$ under variations in k_T' across this boundary.

The degree of continuity of the impact law across the corresponding boundaries is summarized in Table 2 and further illustrated in Fig. 4.

Boundary type	Regions	Continuity
$v_T = 0$ at end of impact phase	1–3, 1–7, 2–4, 2–8	C^0
$v_T = 0$ at end of compression phase	3–5, 4–6, 7–9, 8–10	C^1
$v_T = 0$ at impact; no stick	1–10, 2–9	C^0
$v_T = 0$ at impact; stick	5–6	C^1
Loss of stick phase	3–7, 4–8, 5–9, 6–10	C^0

Table 2
Summarising the degree of continuity of the impact law across each of the 15 different codimension-one boundaries shown in panel (c) of Fig. 4, see text for detailed derivations.

5 Discontinuity-induced bifurcations

For the purpose of this paper, discontinuity-induced bifurcations are those changes in system response that result from the onset of non-generic interactions of an invariant set of a dynamical system with system discontinuities under variation of system parameters [9]. In particular, we restrict attention to codimension-one bifurcations, i.e., non-generic interactions that, without loss of generality, can be unfolded by arbitrarily small variations of a single system parameter.

5.1 Grazing contact

As an example, consider, for some critical parameter value $\eta = \eta^*$, the simple tangential (grazing) contact of a periodic trajectory at a point z^* with the unilateral constraint, i.e., such that $v_N = 0$ and $\dot{v}_N > 0$ in terms of the unscaled variables. In particular, suppose that all other impacts occur with negative normal velocity and with initial conditions for the impact phase away from any of the discontinuity boundaries identified in the previous section.

To investigate the local dynamics in the vicinity of the grazing trajectory and for $\eta \approx \eta^*$, consider the introduction of a local Poincaré section $\Pi = \{v_N = 0\}$ in some neighborhood of z^*. Ignore, for a moment, the presence of the unilateral constraint near z^*. By the transversality of the intersection of the grazing trajectory with Π (since $\dot{v}_N > 0$), it follows that we may define a smooth map P that maps points $z \approx z^*$ on Π to the subsequent intersection near z^* with Π along the corresponding system trajectories with $\eta \approx \eta^*$, such that $P(z^*) = z^*$. Suppose, in particular, that all eigenvalues of the Jacobian of P evaluated at $z = z^*$ and $\eta = \eta^*$ have magnitude distinct from 1. By the assumption of the codimension-one nature of the onset of such contact, it follows that arbitrarily small variations in η result in the persistence of a family of periodic trajectories that intersect Π at points with $z \approx z^*$.

When reintroducing the effects of the unilateral constraints near z^*, the local dynamics in the vicinity of the grazing trajectory and for $\eta \approx \eta^*$ may again be captured by a local map provided that the impact law reduces to the identity in the limit that the unscaled initial normal impact velocity $v_{N,0}$ decays to zero. As can be seen in Fig. 3, initial conditions for the impact phase corresponding to this limit are possible only in regions 1 and 2 and regions 5 and 6 corresponding to impact mappings $\mathbf{g}_I$ and $\mathbf{g}_{III}$, respectively. Indeed, since

$$\lim_{v_{N,0}\to 0} \mathbf{g}_I\left(v_{T,0}, v_{N.0}, k_T, k_N, r\right) = \mathbf{g}_I\left(v_{T,0}, 0, k_T, k_N, r\right) = \left(v_{T,0}, 0\right),$$

the impact law reduces to the identity for points of near-grazing contact with the unilateral constraint and initial states in regions 1 and 2. It follows from the theory of discontinuity mappings introduced by Nordmark [29] (see also [9, Ch. 6]) that the effect of an impact with small unscaled $v_{N,0} < 0$ is to introduce a singularity in the map proportional to $\sqrt{-v_{N,0}}$. The corresponding bifurcation characteristics have been explored at great length by a number of authors and include the possibility of non-smooth folds, robust chaos, period-adding sequences, and universal scaling relationships.

In contrast, for initial states in regions 5 and 6, the onset of grazing contact is catastrophic. Here,

$$\lim_{v_{N,0}\to 0} \mathbf{g}_{III}\left(v_{T,0}, v_{N,0}, k_T, k_N, 0, k_N^0, r\right) = \mathbf{g}_{III}\left(v_{T,0}, 0, k_T, k_N, 0, k_N^0, r\right) = \left(0, r\sqrt{\left(1-\frac{k_N^0}{k_N}\right)\left(\frac{k_N}{k_T}v_{T,0}\right)^2}\right)$$

corresponding to a release velocity an $\mathcal{O}(1)$ distance in the (v_T, v_N) plane away from the initial state. It follows that, generically, a branch of periodic trajectories that intersect Π at points near z^* without experiencing a local impact must terminate at the critical parameter value corresponding to the onset of grazing contact.

5.2 Discontinuities in the impact law

Consider, instead, for some critical parameter values $\eta = \eta^*$, a periodic trajectory with a single, forward-in-time transversal intersection z^* with the unilateral constraint and based at a point $g(z^*)$ on the unilateral constraint, where g represents the corresponding impact law. In particular, suppose that z^* lies on one of the boundaries in the impact law. By transversality it follows that there exists a smooth mapping Q that maps points $z \approx g(z^*)$ at the end of an impact phase to the beginning of the subsequent impact phase along the corresponding system trajectories with $\eta \approx \eta^*$, such that $z^* = (Q \circ g)(z^*)$. The composition $Q \circ g$ then represents a Poincaré mapping that maps points $z \approx z^*$ at the beginning of an impact phase to the beginning of the subsequent impact phase along the corresponding system trajectories with $\eta \approx \eta^*$. In particular, any discontinuities in the impact law are inherited by the Poincaré mapping.

For the 15 distinct boundaries considered in the preceding section, the discontinuity in the impact law (and, consequently, in the Poincaré mapping) is in either the first or the second derivative. The dynamics of piecewise-smooth

mappings of this kind are considered in detail in [9, Chs.3,4]. Specifically, for mappings with a discontinuity in the first derivative, the theory first derived by Feigin (see [11,13]) establishes the existence of two continuous branches of single impact periodic trajectories with impacts on opposite sides of the corresponding boundary, such that each branch exists only on one side of the critical parameter value. If both branches are on the same side of the bifurcation, a *nonsmooth fold* is said to occur; branches being on opposite sides is called a *persistence* scenario. Moreover, the corresponding Floquet multipliers typically converge to different limits as the critical parameter value is approached along the two branches. In contrast, if the jump is in the second derivative of the map, a continuous branch of periodic trajectories exists across the critical parameter value, such that the corresponding Floquet multipliers are continuous but with discontinuous derivatives at $\eta = \eta^*$.

Finally, we also mention the special case where the transition across the boundary causes the gain or loss of an impulsive stick phase at the end of the impact phase. For perturbations that result in impulsive stick, we have a loss of phase space dimension, and the map $Q \circ g$ must develop a Floquet multiplier that is exactly zero.

5.3 Numerical results

To illustrate the analytical results reported above, we consider augmenting the model example from Sec. 2.3 with a specific applied moment and applied forces so as to naturally set up limit cycle oscillations that represent steady vibro-impacting behaviour. The idea is to understand how changes in the velocities at impact as one changes a parameter can affect the dynamic properties of these limit cycles.

The applied forces and moment are here chosen so as to model the dragging of the rod across a moving surface, subject to vertical excitation. Specifically, let $\dot{x} = v_T$, $\dot{y} = v_N$, $\dot{\theta} = \omega$, and

$$\begin{aligned} S_x &= -k_x(x - v_{\mathrm{dr}}t) - c_x(v_T - v_{\mathrm{dr}}) \\ S_y &= -k_y(y - y_0) - c_y((y - y_0)^2 - y_1^2)v_N \\ R &= -k_\theta(\theta - \theta_0) - c_\theta\omega, \end{aligned}$$

where k_x, k_y, k_θ, c_x, c_y, c_θ, y_0, y_1, θ_0, v_{dr}, and the contact parameters μ and r, are constant system parameters. Here, the horizontal force S_x corresponds to a linear spring/damper, but with a reference position that moves with constant velocity v_{dr} (one may, alternatively, consider the system in a frame moving with the reference position, in which case v_{dr} becomes the backward velocity of the ground, as in the case of a moving belt). The torque R again corresponds to a linear spring/damper, with the reference position having a constant offset

θ_0. Finally, the vertical force S_y is that of a van der Pol oscillator, with an offset y_0 and the size of the region of negative damping being y_1. This force gives the system a natural excitation in the vertical direction.

The simple nature of the external time dependence in the system enables us the speak about periodic motion if, after some time T all variables have returned to their original values, except for x which must have increased by the amount $v_{\rm dr}T$. In particular, each row of Tables 3, 4, and 5 corresponds to parameter values and initial conditions (at $t = 0$) for a periodic trajectory with a single, forward-in-time transversal intersection z^* with the unilateral constraint and based at a point $g\,(z^*)$ on the unilateral constraint, where g represents either of the two impact laws on either side of the corresponding boundary. In each subsection below we consider the local dynamics in the vicinity of the periodic trajectory for nearby parameter values $\eta \approx \eta^*$ where the principal bifurcation parameter η is the coefficient of friction μ in Secs. 5.3.1-5.3.3 and Sec. 5.3.5 and $v_{\rm dr}$ in Sec. 5.3.4. Numerical results are quoted in terms of the unscaled variables.

Boundary	r	μ	$v_{\rm dr}$	k_x	k_y	k_θ	c_x	c_y	c_θ	y_0	y_1	θ_0
1–3	1	0.8507	1.8	0.6	1	1.6	0.1	1	0.12	0.5	0.8	0.275π
5–9	1	0.5448	0.2	0.7	1	1.9	0.05	0.05	0.05	0.5	0.8	0.7π
4–6	0.5	0.9355	-0.1	0.7	1	1.9	0.1	0.1	0.1	0.9	1	0.375π
5–6	0.5	0.8	-0.2054	0.7	1	1.9	0.1	0.1	0.1	0.9	1	0.375π
1–10	0.5	0.3495	-0.2	0.7	1	1.9	0.1	0.1	0.1	0.9	1	0.375π

Table 3
Values of system parameters for the different bifurcation examples.

Boundary	x	y	θ	v_T	v_N	ω	T_1	T_2
1–3	-0.7585	0.7032	0.8728	3.2236	-1.5523	-0.0019	0.4014	3.458
5–9	0.0843	0.4948	2.1111	-0.0226	-0.4921	0.1553	5.9219	4.6263
4–6	0.5318	0.7966	2.1871	0.3566	0.9221	-0.1236	5.7325	1.6458
5–6	-0.3734	1.1879	1.3257	-0.3171	0.9486	-0.0071	5.5373	1.8018
1–10	0.2101	0.2747	1.0012	-0.5793	0.5296	0.1281	5.5470	0.5976

Table 4
Initial conditions (at $t = 0$) for the corresponding periodic trajectory, the time T_1 from the initial condition to the subsequent impact, and the time $T_2 = T - T_1$ from the impact back to the initial point, where T is the period.

Boundary	B	μ	$v_{T,0}$
1–3	0.5946	0.9405	1.5692
5–9	−0.5957	0.5957	0.8026
4–6	−0.5926	0.8323	−0.4730
5–6	0.5146	1.1659	0.0000
1–10	0.5165	0.5075	0.0000

Table 5
Values of the scaled impact law variables B, μ, and $v_{T,0}$ at impact.

5.3.1 $v_T = 0$ at end of the impact phase

Consider the periodic single impact trajectory with parameter values and initial conditions given by the first row of Tables 3 and 4 and with an impact on the 1–3 boundary in the impact law. Here,

$$z^* = (0.5534, 0, 0.8691, 3.2869, -1.8947, -0.0149)^T.$$

Substitution into Eq. (12) yields $A = 2.7500$, $B = 1.4790$, $C = 2.2500$ at the beginning of the impact phase, such that $k_T^+ = -.8604$, $k_N^+ = .9918$, $k_T^- = 3.8184$, $k_N^- = 3.5082$, and $k_N^0 = 1.4546$.

The 1–3 boundary in the impact law is characterized by the vanishing of the function

$$H(z,\mu) \stackrel{\text{def}}{=} k_N^+ v_T - (1+r) k_T^+ v_N,$$

where $(z,\mu) \approx (z^*,\mu^*)$ is in region 1 provided that $H(z,\mu) > 0$ and in region 3 otherwise. For nearby points $z \approx z^*$ and parameter values $\mu \approx \mu^*$, it follows that

$$H(z,\mu) = \gamma(z - z^*) + N(\mu - \mu^*) + \mathcal{O}(z - z^*, \mu - \mu^*)^2,$$

where

$$\gamma = \partial_z \left(k_N^+ v_T - (1+r) k_T^+ v_N \right)\Big|_{z=z^*,\mu=\mu^*} = (0, 0, -19.7549, 0.9918, 1.7208, 0),$$
$$N = \partial_\mu \left(k_N^+ v_T - (1+r) k_T^+ v_N \right)\Big|_{z=z^*,\mu=\mu^*} = -15.2820.$$

Initial conditions $z \approx z^*$ in region 1 correspond to a *Case I* impact phase with rate constants k_T^+ and k_N^+, while those in region 3 correspond to a *Case II* impact phase with rate constants k_T^+, k_N^+, k_T^0, and k_N^0. From Eq. (19) it follows that

$$\delta \left[\mathbf{g}_{II} \left(v_T, v_N, k_T^+, k_N^+, k_T^0, k_N^0, r \right) - \mathbf{g}_I \left(v_T, v_N, k_T^+, k_N^+, r \right) \right]$$
$$= \left[(-1.0082, -0.5423) + \mathcal{O}(\delta z) \right] \delta \left(k_N^+ v_T - (1+r) k_T^+ v_N \right)$$

for $z \approx z^*$. Let g_1 and g_3 denote the impact laws on the corresponding sides of the 1–3 boundary. From (10) it follows that

$$\left.\frac{d(g_3 - g_1)}{d\left(k_N^+ v_T - (1+r)k_T^+ v_N\right)}\right|_{z=z^*,\mu=\mu^*} = (0,0,0,-1.0082,-0.5423,0.8401)^T .$$

To $\mathcal{O}(z-z^*, \mu-\mu^*)$ the composite Poincaré mapping now takes the form

$$(Q \circ g)(z,\mu) = \begin{cases} \alpha(z-z^*) + M(\mu-\mu^*) & \text{if} \quad H(z,\mu) > 0 \\ \alpha(z-z^*) + M(\mu-\mu^*) + \beta H(z,\mu) & \text{if} \quad H(z,\mu) < 0 \end{cases}, \quad (21)$$

where

$$\begin{aligned} \alpha &= \partial_z Q|_{z=g_1(z^*),\mu=\mu^*} \cdot \partial_z g_1|_{z=z^*,\mu=\mu^*} , \\ \beta &= \partial_z Q|_{z=g_1(z^*),\mu=\mu^*} \cdot \left.\frac{d(g_3 - g_1)}{d\left(k_N^+ v_T - (1+r)k_T^+ v_N\right)}\right|_{z=z^*,\mu=\mu^*} , \\ M &= \partial_z Q|_{z=g_1(z^*),\mu=\mu^*} \cdot \partial_\mu g_1|_{z=z^*,\mu=\mu^*} + \partial_\mu Q|_{z=g_1(z^*),\mu=\mu^*} . \end{aligned}$$

Numerical values of the matrices are

$$\partial_z Q|_{z=g_1(z^*),\mu=\mu^*} = \begin{pmatrix} -0.8058 & -0.9081 & -0.4528 & 0.1679 & 0.1828 & -0.0607 \\ 0 & 0 & 0 & 0 & 0 & 0 \\ 0 & 0.0091 & -0.2368 & 0 & -0.0018 & 0.1924 \\ -0.1007 & 0.0198 & 0.7254 & -0.8226 & -0.0040 & -0.4394 \\ 0 & 0.0132 & 0.9750 & 0 & -0.0357 & 0.3378 \\ 0 & 0.0119 & -0.9221 & 0 & -0.0024 & -0.3051 \end{pmatrix},$$

$$\partial_\mu Q|_{z=g_1(z^*),\mu=\mu^*} = (0,0,0,0,0,0)^T$$

and

$$\partial_z g_1|_{z=z^*,\mu=\mu^*} = \begin{pmatrix} 1 & 0 & 0 & 0 & 0 & 0 \\ 0 & 1 & 0 & 0 & 0 & 0 \\ 0 & 0 & 1 & 0 & 0 & 0 \\ 0 & 0 & -19.9170 & 1 & 1.7348 & 0 \\ 0 & 0 & 0 & 0 & -1 & 0 \\ 0 & 0 & 15.1707 & 0 & -0.0255 & 1 \end{pmatrix},$$

$$\partial_\mu g_1|_{z=z^*,\mu=\mu^*} = (0,0,0,-15.4075,0,8.8257)^T .$$

By the Feigin theory,

$$1 - \gamma(I - \alpha)^{-1}\beta = -0.7594 < 0$$

implies that the two branches of periodic single impact trajectories with impacts in regions 1 and 3, respectively, exist on the same side of $\mu = \mu^*$. This is a nonsmooth fold. Indeed, since

$$N + \gamma(I - \alpha)^{-1}M = 5.0087 > 0,$$

these branches exist for $\mu > \mu^*$ (cf. panel (a) of Fig. 6).

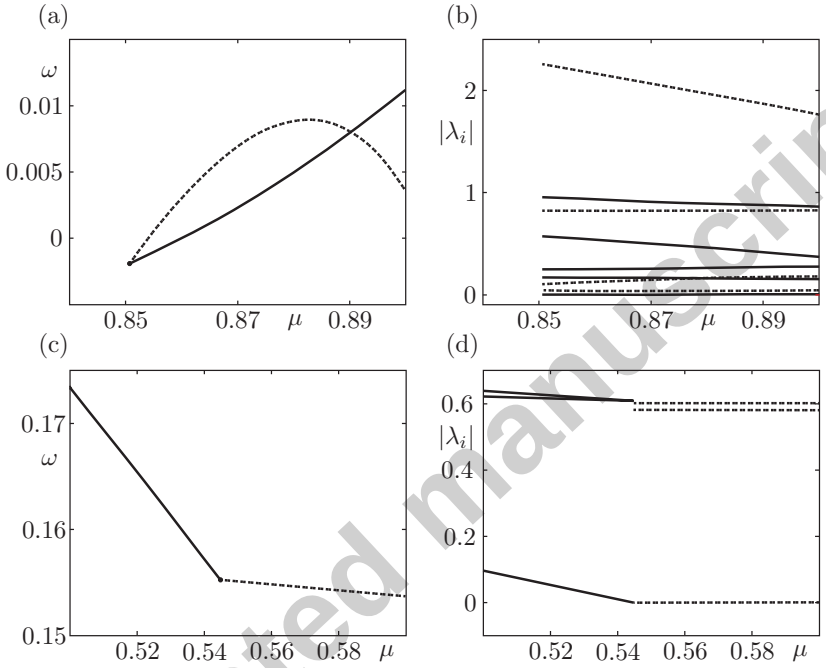

Fig. 6. (a) Variations in ω on the Poincaré section $\Pi : \{x - v_{\rm dr}t = -0.7585\}$ along two branches of region 3 (solid) and region 1 (dashed) impacting periodic trajectories that emanate from a non-smooth fold; (b) Absolute values of the corresponding characteristic multipliers; (c) Variations in ω on the Poincaré section $\Pi : \{x - v_{\rm dr}t = 0.0843\}$ along two branches of region 9 (solid) and region 5 (dashed) impacting periodic trajectories that emanate from a persistent bifurcation; (d) Absolute values of a subset of the corresponding characteristic multipliers.

As seen in panel (b) of Fig. 6, the trajectory with impacts in region 3 is asymptotically stable for $\mu \approx \mu^*$, while the trajectory with impacts in region 1 is unstable. In agreement with the theory, the Floquet multipliers are discontinuous functions of μ at $\mu = \mu^*$ and the trajectory with impact in region 3 has one Floquet multiplier equal to zero corresponding to a final impulsive stick segment during the impact phase. The piecewise linear approximation of the Poincaré map can be further used to explore the existence of additional

branches of periodic trajectories. Here, it was found, that other than the two branches of single-impact periodic trajectories, no periodic trajectories with 10 or fewer impacts per period exist on some neighborhood of the critical parameter trajectory and for $\mu \approx \mu^*$.

5.3.2 Loss of stick phase

Consider, instead, the periodic single-impact trajectory with an impact on the 5–9 boundary in the impact law and obtained with the parameter values and initial conditions given by the second row of Tables 3 and 4. Here,

$$z^* = (0.1155, 0, 2.2817, 0.2852, -0.3250, -0.1314)^T .$$

Substitution into Eq. (12) yields $A = 2.7227$, $B = -1.4834$, $C = 2.2773$ at the beginning of the impact phase, such that $k_T^+ = -2.9667$, $k_N^+ = 3.0855$, $k_T^- = 0$, $k_N^- = 1.4692$, and $k_N^0 = 1.4692$.

The 5–9 boundary in the impact law is characterized by the vanishing of the function

$$H(z, \mu) \stackrel{\text{def}}{=} k_T^-.$$

For nearby points $z \approx z^*$ and parameter values $\mu \approx \mu^*$, it follows that

$$H(z, \mu) = \gamma(z - z^*) + N(\mu - \mu^*) + \mathcal{O}(z - z^*, \mu - \mu^*)^2,$$

where

$$\gamma = \partial_z k_T^-\Big|_{z=z^*,\mu=\mu^*} = (0, 0, -2.0616, 0, 0, 0),$$
$$N = \partial_z k_T^-\Big|_{z=z^*,\mu=\mu^*} = 2.7227.$$

Initial conditions $z \approx z^*$ in region 5 correspond to a *Case III* impact phase with rate constants k_T^+, k_N^+, 0, and k_N^0 while those in region 9 correspond to a *Case III* impact phase with rate constants k_T^+, k_N^+, k_T^-, and k_N^-. From Eq. (20) it follows that

$$\delta\left[\mathbf{g}_{III}\left(v_T, v_N, k_T^+, k_N^+, k_T^-, k_N^-, r\right) - \mathbf{g}_{III}\left(v_T, v_N, k_T^+, k_N^+, 0, k_N^0, r\right)\right] = \left[(0.1726, -0.0411) + \mathcal{O}(\delta z)\right]\delta k_T^-$$

for $z \approx z^*$. Let g_5 and g_9 denote the impact laws on the corresponding sides of the 5–9 boundary. From Eqs. (10) it follows that

$$\left.\frac{d(g_9 - g_5)}{d\left(k_N^-\right)}\right|_{z=z^*,\mu=\mu^*} = (0, 0, 0, 0.1725, -0.0411, -0.1182)^T .$$

The composite Poincaré mapping now again takes the form of Eq. (21), where

$$\partial_z Q|_{z=g_1(z^*),\mu=\mu^*} = \begin{pmatrix} 0.1799 & 0.2610 & 0.2170 & -1.0017 & -0.1009 & -0.9636 \\ 0 & 0 & 0 & 0 & 0 & 0 \\ 0 & -0.4030 & 0.2710 & 0 & 0.1558 & 0.0530 \\ 0.7012 & 1.3776 & 1.0600 & 0.2300 & -0.5326 & 0.9518 \\ 0 & 1.0280 & -2.1653 & 0 & 0.7637 & -0.4606 \\ 0 & -1.3828 & -0.6842 & 0 & 0.5346 & -0.7568 \end{pmatrix},$$

$$\partial_\mu Q|_{z=g_1(z^*),\mu=\mu^*} = (0,0,0,0,0,0)^T$$

and

$$\partial_z g_5|_{z=z^*,\mu=\mu^*} = \begin{pmatrix} 1 & 0 & 0 & 0 & 0 & 0 \\ 0 & 1 & 0 & 0 & 0 & 0 \\ 0 & 0 & 1 & 0 & 0 & 0 \\ 0 & 0 & 0 & 0 & 0 & 0 \\ 0 & 0 & -0.0226 & -0.0686 & -0.7532 & 0 \\ 0 & 0 & 0.1620 & 0.5348 & -0.8579 & 1 \end{pmatrix},$$

$$\partial_\mu g_5|_{z=z^*,\mu=\mu^*} = (0,0,0,0,-0.0447,-0.0219)^T.$$

By the Feigin theory

$$1 - \gamma(I-\alpha)^{-1}\beta = 0.9402 > 0$$

implies that the two branches of periodic single impact trajectories with impacts in regions 5 and 9, respectively, exist on opposite sides of $\mu = \mu^*$. This is a persistence scenario. Indeed, since

$$N + \gamma(I-\alpha)^{-1}M = 2.7448 > 0,$$

the branch of periodic trajectories with impacts in region 5 exists for $\mu > \mu^*$, while the branch of periodic trajectories with impacts in region 9 exists for $\mu < \mu^*$ (cf. panel (c) of Fig. 6). As the corresponding periodic trajectories are asymptotically stable for $\mu \approx \mu^*$, it follows that this bifurcation scenario corresponds to the persistence of a local attractor.

As seen in panel (d) of Fig. 6, one of the Floquet multipliers of the periodic trajectory with impacts in region 5 again equals zero, corresponding to a impacting stick segment at the conclusion of the impact phase. This multiplier

connects continuously to a nonzero multiplier for the periodic trajectory with impacts in region 9, while all other multipliers experience discontinuous, but relatively small, jumps at $\mu = \mu^*$. Indeed, Eq. (20) shows that the difference in linearization of the impact law between regions 5 and 9 evaluated at $z = z^*$ and $\mu = \mu^*$ is proportional to the gradient of k_T^- with respect to z evaluated at $z = z^*$ and $\mu = \mu^*$. As k_T^- depends only on q and not on $\dot{q}$, this gradient is nonzero only in those components that relate to differentiation with respect to q. On the other hand, the linearization of the impact law in region 5 evaluated at $z = z^*$ and $\mu = \mu^*$ has a left nullvector that is nonzero only in those components that relate to differentiation with respect to $\dot{q}$ (the impact law is the identity for q). It follows that this nullvector is also a left nullvector for the linearization of the impact law in region 9 evaluated at $z = z^*$ and $\mu = \mu^*$ explaining the existence of a zero Floquet multiplier for the latter impact law in this limit.

The piecewise linear approximation of the Poincaré map can again be used to explore the existence of additional branches of periodic trajectories. Here, it was found that, other than the two branches of single-impact periodic trajectories, no periodic trajectories with 10 or fewer impacts per period exist on some neighborhood of the critical periodic trajectory and for $\mu \approx \mu^*$.

5.3.3 $v_T = 0$ at end of compression phase

Now consider the periodic single impact orbit with an impact on the 4–6 boundary in the impact law obtained with the corresponding parameter values and initial conditions in Tables 3 and 4. The Poincaré mapping is piecewise smooth with a continuous first derivative and it follows that the periodic trajectory persists for $\mu \approx \mu^*$ with continuously varying Floquet multipliers albeit with a discontinuous slope at $\mu = \mu^*$ (cf. panels (a) and (b) of Fig. 7).

5.3.4 $v_T = 0$ at impact; stick

Now consider the periodic single impact orbit with an impact on the 5–6 boundary in the impact law obtained with the corresponding parameter values and initial conditions in Tables 3 and 4. The Poincaré mapping is piecewise smooth with a continuous first derivative and it follows that the periodic trajectory persists for $v_{\mathrm{dr}} \approx v_{\mathrm{dr}}^*$ with continuously varying Floquet multipliers albeit with a discontinuous slope at $v_{\mathrm{dr}} = v_{\mathrm{dr}}^*$ (cf. panel (c) of Fig. 7).

5.3.5 $v_T = 0$ at impact; no stick

Finally, consider the periodic single impact orbit with an impact on the 1–10 boundary in the impact law obtained with the corresponding parameter values

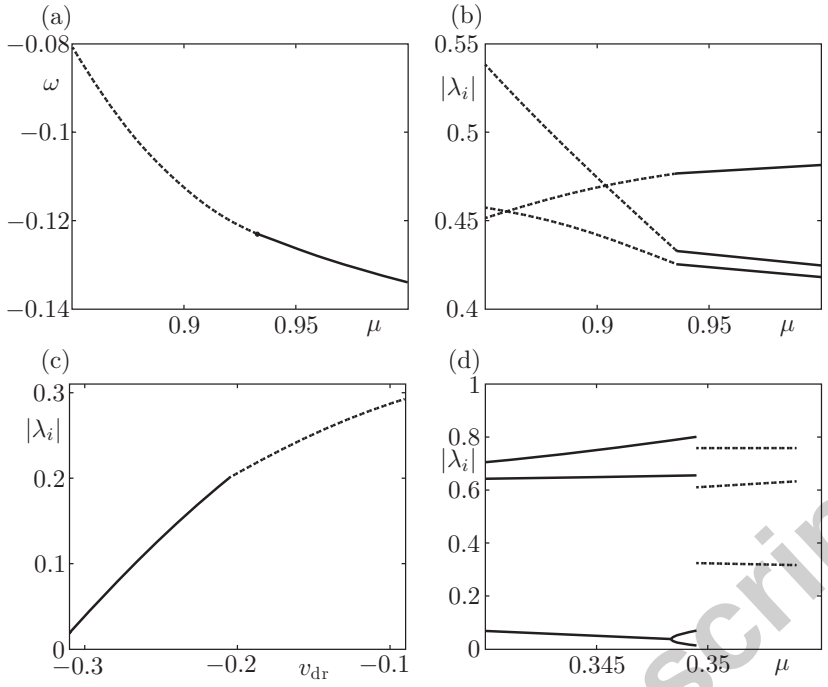

Fig. 7. (a) Variations in ω on the Poincaré section $\Pi : \{x - v_{\rm dr}t = 0.5318\}$ along two branches of region 6 (solid) and region 4 (dashed) impacting periodic trajectories that emanate from a persistent bifurcation; (b) Absolute values of a subset of the corresponding characteristic multipliers; (c) Variations in the absolute value of one of the characteristic multipliers along two branches of region 6 (solid) and region 5 (dashed) impacting periodic trajectories that emanate from a persistent bifurcation. (d) Variations in the absolute value of the characteristic multipliers along two branches of region 10 (solid) and region 1 (dashed) impacting periodic trajectories that emanate from a persistent bifurcation.

and initial conditions in Tables 3 and 4. The Poincaré mapping is piecewise smooth with a discontinuous first derivative. The analysis undertaken in a previous section may again be repeated so as to allow for the application of the Feigin theory for piecewise-linear mappings with a discontinuous linearization on the boundary. As seen in panel (d) of Fig. 7, the branch of periodic trajectories with impacts in region 1 exists for $\mu > \mu^*$, while the branch of periodic trajectories with impacts in region 10 exists for $\mu < \mu^*$. As the corresponding periodic trajectories are asymptotically stable for $\mu \approx \mu^*$, it follows that this bifurcation scenario corresponds to the persistence of a local attractor. As predicted by the theory, no Floquet multipliers are continuous at $\mu = \mu^*$. No periodic trajectories with 10 or fewer impacts per period exist on some neighborhood of the critical periodic trajectory and for $\mu \approx \mu^*$.

6 Discussion

At the core of the present paper is a discrete impact law that models the change in the generalized velocities of a planar rigid-body mechanism following a collisional interaction of elements of the mechanism with the surrounding environment (or, with some modification, with each other). The derivation of this impact law relies heavily on the following set of consistent assumptions, see e.g., [1,2,38].

Orders of magnitude: As discussed in Sec. 2.2, the contact phase occurs over a time scale that is asymptotically shorter than the typical time scale of the macroscopic behavior of the rigid-body mechanism. In particular, while the normal and tangential contact forces are assumed to be an order of magnitude larger than those forces acting on the mechanism from sources other than the contact, the integrated normal and tangential impulses across the contact phase are finite. By a suitable rescaling, this assumption results in a closed set of differential equations governing the rates of change of the relative tangential and normal velocities at the contact point in terms of the normal and tangential forces during the contact phase and in terms of constant coefficients that can be expressed as functions of the generalized coordinates at the onset of the contact phase. Moreover, in the present case of planar mechanical systems, these differential equations can be solved in closed form.

Segment decomposition: The normal and tangential contact forces are assumed to obey the assumptions of the classical Amonton-Coulomb model of dry friction. This results in a decomposition of the impact phase into distinct segments of motion during which the contact point is in slip (in either tangential direction) or in stick. This allows for the modeling of impact phases that include a change of the direction of tangential motion. It also encompasses the Painlevé phenomenology whereby the normal velocity initially increases as a result of the onset of contact (see panels (b) and (c) of Fig. 3).

Dissipation: The net change in kinetic energy of the rigid-body mechanism across the impact phase is nonpositive. In particular, the impact phase is resolved into a compressive phase during which the normal velocity results in an increased depth of relative normal penetration and a restitutive phase during which the relative normal motion is in the direction of reduced penetration. Here, only a fraction of the negative work performed by the normal contact force during the compressive phase is returned as positive work to the mechanism during the restitutive phase. Moreover, as the tangential contact force is opposite in direction to the relative tangential motion during slip, the resultant work is always nonpositive.

The derivation of the impact law presented here is entirely equivalent to that

presented in the work of Stronge [38]. The specific new contributions here are i) a detailed enumeration of explicit expressions for the relative normal and tangential velocities at the end of the impact phase in terms of their values at the onset of contact; ii) a detailed enumeration of the boundaries between regions of initial conditions and parameter values that result in distinct expressions for the impact law; and iii) a detailed enumeration of the smoothness properties of the impact law across these boundaries. This formulation is designed to enable implementation of the impact law in hybrid forward-simulation integration algorithms, and is also suitable for unfolding discontinuity-induced bifurcations.

In particular, several of the impact law boundaries were shown to be associated with discontinuities in the first derivative of the impact law. As supported by explicit numerical calculations, the Feigin theory for piecewise-linear maps [11,9,13] can then be successfully applied to analyse the case of a limit cycle trajectory that impacts on such a boundary. Specifically, the persistence and stability properties of branches of periodic orbits that emanate from such a bifurcation point can be rigorously established. Of particular importance to applications is the demonstration of the existence of nonsmooth folds along such branches, which correspond to the sudden loss of a local attractor in the system response under parameter variation. The phenomenology developed generalizes to arbitrary rigid-body mechanisms, provided that the particular impact law boundaries are realizable given physically realistic system parameters. For example, in the model example discussed above, the Painlevé phenomenon occurs only for values of $\mu > 4/3$.

Alternative formulations of impact laws have a long history and continue to be cited and applied in the literature. These include the classical Newton *kinematic coefficient of restitution* equal to the negative ratio of the relative normal velocities before and after the contact phase and the Poisson *kinetic coefficient of restitution* equal to the ratio between the normal impulses during restitution and compression (see Keller [21] and Pfeiffer and Glocker [34]). For smooth contact (i.e., when $\mu = 0$ in our present notation), the kinematic, kinetic, and energetic coefficients of restitution are equivalent and predict the same release velocities.

In the case of impacts with friction, the kinematic approach can be generalised to include a second, tangential coefficient of restitution equal to the negative ratio of the relative tangential velocities before and after the contact phase (see Walton [42] and Payr & Glocker [32]). In general, however, the kinematic, kinetic, and energetic approaches do not agree for impacts with friction, unless the impact phase is such that the direction of relative tangential motion is constant (Case I in Sec. 3.2 above). Indeed, as discussed further by both Batlle [1] and Stronge [38] (see also the review paper [37]) both the kinematic and kinetic formulations suffer from the problem that in some cases they predict

a non-physical *increase* in the kinetic energy of the rigid-body mechanism as a result of the collision.

In addition to agreed-upon first principles, including the dissipative nature of collisional contact, proposed impact laws may be evaluated in terms of their agreement with suitable limits of models of compliant contact. For example, in [39] it is shown that models employing kinematic coefficients of restitution do not agree with the infinite-stiffness limit of predictions made from models that rely on a combination of dry friction and tangential and normal compliance and that allow for changes in the direction of relative slip during the contact phase. In contrast, the rigid-body impact laws formulated here are consistent with the predictions of such models.

A wider goal than that achieved here is to enumerate and analyse all codimension-one discontinuity-induced bifurcations in the system response that result from a consistent hybrid formulation of rigid-body mechanics in the presence of impacts, sustained contact, and dry friction, in the manner of the ongoing program of work for other classes of piecewise-smooth dynamical systems [9,10,13]. Future work will determine whether one can unfold, in a consistent way, the ambiguities inherent in rigid-body formulations with impact and friction, collectively known as Painlevé paradoxes [16,24,31,37], without moving to compliant formulations.

It should also be remembered that the analysis presented here has been restricted to planar motion with isolated points of contact. In the case of three-dimensional motion with isolated points of contact, a similar approach might be applicable (see [3]), but closed-form expressions for the impact mappings are no longer available. Future work will consider extending the formulation to analyze discontinuity-induced bifurcations in the three-dimensional case. It should also be stressed that situations with simultaneous contact at multiple points or along contact lines cannot currently be resolved within the present framework.

7 Acknowledgment

We thank the CRM at UAB Barcelona for their hospitality during the thematic program on piecewise-smooth systems in Spring 2007. This material is based upon work supported by the U.S. National Science Foundation under Grant No. 0635469, and by the UK EPSRC.

References

[1] J.A. Batlle, On Newton's and Poisson's Rules of Percussive Dynamics, Journal of Applied Mechanics, 60 (1993), 376-381.

[2] J.A. Batlle, The sliding velocity flow of rough collisions in multibody systems, ASME Journal of Applied Mechanics 63 (1996) 804–809.

[3] J.A. Batlle, Termination conditions for three-dimensional inelastic collisions in multibody systems, Int J. Impact Eng. 25 (2001), 615–629.

[4] B. Brogliato, Nonsmooth Mechanics – Models, Dynamics and Control, Springer-Verlag, 1999.

[5] C.J. Budd and F. Dux, Chattering and related behaviour in impact oscillators, Philos. Trans. R. Soc. A-Math. Phys. Eng. Sci. 347 (1994) 365–389.

[6] H. Dankowicz and A.B. Nordmark, On the origin and bifurcations of stick-slip oscillations, Physica D 136 (2000) 280–302.

[7] H. Dankowicz and X. Zhao, Local analysis of co-dimension-one and co-dimension-two grazing bifurcations in impact microactuators, Physica D 202 (2005) 238-257.

[8] M. di Bernardo, C.J. Budd, and A.R. Champneys, Normal form maps for grazing bifurcations in n-dimensional piecewise-smooth dynamical systems, Physica D 160 (2001) 222–254.

[9] M. di Bernardo, C.J. Budd, A.R. Champneys and P. Kowalczyk, Piecewise-Smooth Dynamical Systems; theory and applications Springer-Verlag, New York, 2007.

[10] M. di Bernardo, C.J. Budd, A.R. Champneys, P. Kowalczyk, A.B. Nordmark, G. Olivar Tost, and P.T. Piiroinen, Bifurcations in nonsmooth dynamical systems, SIAM Rev. 50 (2008) 629–701.

[11] M. di Bernardo, M.I. Feigin, S.J. Hogan, and M.E. Homer, Local analysis of C-bifurcations in n-dimensional piecewise-smooth dynamical systems, Chaos Solitons Fractals 10 (1999) 1881–1908.

[12] M. di Bernardo, P. Kowalczyk, and A. Nordmark, Bifurcations of dynamical systems with sliding: Derivation of normal-form mappings, Physica D 170 (2002) 175–205.

[13] M.I. Feigin, Forced Oscillations in systems with discontinuous nonlinearities, (in Russian) Nauka, Moscow, 1994.

[14] A.F. Filippov, Differential Equations with Discontinuous Righthand Sides, Kluwer, Dortrecht, 1988.

[15] M.H. Fredriksson and A.B. Nordmark, Bifurcations caused by grazing incidence in many degrees of freedom impact oscillators, Proc. R. Soc. A-Math. Phys. Eng. Sci. 453 (1997) 1261–1276.

[16] F. Génot and B. Brogliato, New results on Painlevé paradoxes, Eur. J. Mech. A-Solids 18 (1999) 653–677.

[17] J. Guckenheimer and P. Holmes, Nonlinear Oscillations, Dynamical Systems, and Bifurcations of Vector Fields, Springer-Verlag, New York, 1983.

[18] W.P.M.H. Heemels and B. Brogliato, The complementarity class of hybrid dynamical systems, Eur. J. Control 9 (2003) 332–360.

[19] A.P. Ivanov, Energetics of a collision with friction, J. Applied Math. Mech., 56 (1992) 527-534.

[20] W. Kang, P. Thota, B. Wilcox, and H. Dankowicz, Bifurcation analysis of a microactuator using a new toolbox for continuation of hybrid system trajectories, J. Comput. Nonlinear Dyn.-Trans. ASME 4 (2009) 011009 1–8.

[21] J.B. Keller, Impact with friction, J. Appl. Mech.-Trans. ASME 53 (1986) 1–4.

[22] Yu.A. Kuznetsov, Elements of Applied Bifurcation Theory (3rd edition) Springer-Verlag, New York, 2002.

[23] G. Lancioni, S. Lenci, and U. Galvanetto, Non-linear dynamics of a mechanical system with a frictional unilateral constraint, to appear in Int. J. Non-Linear Mech. (2009).

[24] R.I. Leine, B. Brogliato and H. Nijmeijer, Periodic motion and bifurcations induced by the Painlevé paradox, Eur. J. Mech. A-Solids 21 (2002) 869–896.

[25] R.I. Leine and H. Nijmeijer, Dynamics and Bifurcations in Non-Smooth Mechanical Systems, Springer-Verlag, New York, 2004.

[26] I. Merillas, U. Galvanetto and C. Batlle. Sliding bifurcations in a stick-slip system, preprint.

[27] J.J. Moreau, Differential measures of vector functions and some evolution problems, C. R. Acad. Sci. Paris A 282 (1976) 837–840.

[28] J.J. Moreau and P.D. Panagiotopoulos, Nonsmooth Mechanics and Applications, CISM Courses and Lectures 302, Springer-Verlag, New York, 1988.

[29] A.B. Nordmark, Non-periodic motion caused by grazing incidence in an impact oscillator, J. Sound Vibr. 145 (1991) 279–297.

[30] A.B. Nordmark and P.T. Piiroinen, Simulation and stability analysis of impacting systems with complete chattering, to appear in Nonlinear Dyn. (2009).

[31] P. Painlevé, Sur les lois due forttement de glissement, Comptes Rendu des Séances de l'Academie des Sciences 141 (1905) 401–405, 546–552.

[32] M. Payr and C. Glocker, Oblique frictional impact of a bar: Analysis and comparison of different impact laws, Nonlinear Dyn. 41 (2005) 361–383.

[33] P.T. Piiroinen and Yu. A. Kuznetsov, An event-driven method to simulate Filippov systems with accurate computing of sliding motions, ACM Trans. Math. Softw. 34 (2008) 13:1–24.

[34] F. Pfeiffer and C. Glocker, Multibody dynamics with unilateral contacts John Wiley, Chichester, 1996.

[35] K. Popp and P. Stelter, Stick-slip vibrations and chaos, Philos. Trans. R. Soc. A-Math. Phys. Eng. Sci. 332 (1990) 89–105.

[36] S.N. Simic, K.H. Johansson, J. Lygeros, and S. Sastry, Towards a geometric theory of hybrid systems, Dyn. Contin. Discret. Impulsive Syst. B 12 (2005) 649–687.

[37] D.E. Stewart, Rigid-body dynamics with friction and impacts, SIAM Rev. 42 (2000) 3–39.

[38] W.J. Stronge, Impact Mechanics, Camridge University Press, Cambridge, 2000.

[39] W.J. Stronge, R. James and B. Ravani, Oblique impact with friction and tangential compliance, Philos. Trans. R. Soc. A-Math. Phys. Eng. Sci. 359 (2001) 2447–2465.

[40] F. Svahn and H. Dankowicz, Energy transfer in vibratory systems with friction exhibiting low-velocity collisions. J. Vib. Control 14 (2008) 255–284.

[41] P. Thota and H. Dankowicz, TC-HAT: A novel toolbox for the continuation of periodic trajectories in hybrid dynamical systems, SIAM J. Appl. Dyn. Syst. 7 (2007) 1283–1322.

[42] O.R. Walton, Numerical simulation of inelastic, frictional particle-particle interaction, in: M. C. Roco (Ed.), Particulate Two-Phase Flow, Butterworth-Heinemann, New York, 1992, pp. 884-911.

[43] X. Zhao and H. Dankowicz, Unfolding degenerate grazing dynamics in impact actuators, Nonlinearity 19 (2006) 399-418.